Journal of Advanced Research in Applied Sciences and Engineering Technology

Journal homepage:
https://semarakilmu.com.my/journals/index.php/applied_sciences_eng_tech/index
ISSN: 2462-1943

Microwave-Assisted Sonochemical Synthesis of Copper Oxide Nanostructures: Optimization of Seed Layer Number and Low Microwave Power for Enhanced Morphological, Structural, and Optical Properties

Zahidah Othman[1,2], Nur Fairuz Rostan[1,2], Maryam Mohammad[1,2,3], Nur Atiqrah Khairul Azhar[1,2], Mohamad Dzulfiqar Bakri[1,2], Kevin Alvin Eswar[1,2,5], Irmaizatussyehdany Buniyamin[1,2], Mohamad Hafiz Mamat[4], Mohd Husairi Fadzilah Suhaimi[1,2], Rosdiyana Hisam[2], Tetsuo Soga[6], Mohd Firdaus Malek[1,2,*]

[1] NANO-SciTech Lab (NST), Centre for Functional Materials & Nanotechnology (CFMN), Institute of Science, Universiti Teknologi MARA, 40450, Shah Alam, Selangor, Malaysia
[2] School of Physics and Materials Studies, Faculty of Applied Sciences, Universiti Teknologi MARA, 40450 Shah Alam, Selangor, Malaysia
[3] Department of Physics, Faculty of Applied Sciences, Universiti Teknologi MARA (UiTM), Perak Branch, Tapah Campus, Tapah Road, 35400 Perak, Malaysia
[4] NANO-ElecTronic Centre (NET), Faculty of Electrical Engineering, Universiti Teknologi MARA (UiTM), 40450 Shah Alam, Selangor, Malaysia
[5] Faculty of Applied Sciences, Universiti Teknologi MARA (UiTM), Sabah Branch Tawau Campus, 91032 Tawau, Malaysia
[6] Department of Electrical and Mechanical Engineering, Nagoya Institute of Technology (NITech), Showa-ku, Gokiso-cho, Nagoya, 466-8555, Japan

ARTICLE INFO

Article history:
Received 10 February 2026
Received in revised form 30 May 2026
Accepted 2 June 2026
Available online 14 August 2026

Keywords:
Cupric oxide; CuO; Sonochemical; Microwave; Nanostructures; Nanoflowers

ABSTRACT

Copper oxide (CuO), a transition metal oxide, has garnered significant attention due to its versatile properties and potential applications in batteries, magnetic storage, gas sensors, supercapacitors, catalysts, antimicrobials, solar cells, and superconductors. CuO is especially promising owing to its narrow bandgap (1.2 eV), environmental friendliness, low cost, and ease of fabrication. This study investigates the structural and optical properties of CuO films synthesized via a microwave-assisted sonochemical process on fluorine-doped tin oxide (FTO) glass substrates coated with a seeded catalyst layer. The influence of varying seed layer numbers and low microwave power settings (P10, P20, and P30) on the morphology, crystallinity, and optical behavior of the nanostructured CuO thin films was systematically examined. Morphological analysis was conducted using Field Emission Scanning Electron Microscopy (FESEM), crystallinity and chemical bonding were characterized by X-ray diffraction (XRD), and optical properties were assessed via UV-Vis-NIR spectroscopy. Results demonstrate successful formation of CuO nanostructures (Ns) with enhanced properties under optimized low microwave power conditions, confirming the effectiveness of the microwave-assisted sonochemical technique for CuO synthesis.

[*] *Corresponding author.*
E-mail address: mfmalek07@uitm.edu.my*; mfmalek07@gmail.com*

1. Introduction

Copper oxide nanostructured materials have attracted significant interest due to their unique properties and potential applications in optics, optoelectronics, catalysis, gas sensors, and solar cells. Transition metal oxide nanostructures (Ns) such as copper oxide (CuO), iron oxide (Fe_2O_3), and zinc oxide (ZnO) exhibit distinct chemical and physical characteristics compared to their bulk counterparts, primarily due to quantum size effects and their large specific surface areas [1]. CuO exists mainly in two forms: cupric oxide (CuO) and cuprous oxide (Cu_2O), both p-type semiconductors where holes are the primary charge carriers. This p-type behavior arises from copper vacancies or excess oxygen, enabling applications in p-n junctions, gas sensors, and solar devices where hole conduction is crucial. CuO has a narrow bandgap and strong visible light absorption, with optical direct band gaps ranging from 1.3 to 3.7 eV for CuO and 1.8 to 2.5 eV for Cu_2O. Kim and Lee described CuO as a charge-transfer or Mott insulator due to its strong electron correlations [2]. Owing to its monoclinic structure and high surface reactivity, CuO exhibits significant oxygen absorption, making it suitable for catalysis, photocatalysis, sensors, photovoltaic cells, batteries, electrochromic devices, superconductors, magnetic storage, solar cells, and field emission applications [3-8]. Both CuO and Cu_2O are effective catalysts for environmental reactions, including pollution degradation and gas conversion, owing to their oxygen absorption and reactivity [9, 10]. Compared to Cu_2O, CuO offers broader light absorption into the near-infrared region and demonstrates superior electrical conductivity and stability, making it a more reliable nanomaterial for various applications [10-12]. However, CuO's efficiency is limited by low carrier concentration, high resistivity, and recombination rates [13].

Despite its promise, research on the surface properties of CuO thin films remains limited. Controlling the morphological and structural features of CuO Ns such as particle size, crystallinity, and surface area during synthesis remains challenging, particularly using microwave methods. These parameters critically influence the film's performance, but optimization techniques are not yet well-established. Understanding the relationships between CuO thin film structure, morphology, and resulting physical and chemical properties is essential for tuning materials for targeted applications [14, 15]. Recently, interest has surged in synthesizing CuO Ns with diverse morphologies using various methods including electrodeposition, electron beam evaporation, magnetron sputtering, molecular beam epitaxy, sol-gel, solution growth, spin coating, successive ionic layer adsorption and reaction (SILAR), thermal evaporation, and vapor deposition [16-20]. However, conventional techniques such as sol-gel, co-precipitation, and thermal decomposition often suffer from long processing times, high energy consumption, poor control over particle size and shape, and reproducibility issues. These drawbacks limit scalability and reduce effectiveness in advanced applications such as photocatalysis, optoelectronics, and sensing [21]. To address these challenges, this study explores the microwave-assisted sonochemical synthesis of CuO Ns, offering rapid, energy-efficient processing with enhanced control over morphology. The focus is on optimizing seed layer number and microwave power (P10-P30) to produce CuO thin films with improved morphological, structural, and optical properties.

2. Materials and Methods

2.1 Preparation of CuO seed layers

Initially, seed layers (SLs) of copper oxide nanoparticles (CuO NPs), designated as SL 1 and SL 2, were deposited onto fluorine-doped tin oxide (FTO) glass substrates using the spin coating technique. This method aimed to compare the morphological and structural differences in the resulting CuO NP thin films. The CuO SLs were prepared systematically to ensure optimal thin-film properties. The seed

layer on the FTO glass promotes uniform nucleation, enhances adhesion, controls nanostructure orientation, and improves the overall quality and performance of the CuO thin films. The preparation of the CuO NP seed layer solution was carried out with minor modifications based on the method reported by Deka et al. [22]. In a 100 mL container, 20 mL of methanol (CH_3OH), 10 mM of ethanolamine (C_2H_7NO), and 5 mM of copper(II) acetate [$Cu(CH_3COO)_2$] were combined to prepare the precursor solution. In this formulation, 2-methoxyethanol served as the solvent, ethanolamine as the stabilizer, and copper(II) acetate as the precursor. The solution was stirred continuously for 30 minutes on a hotplate at 80 °C, with the stirring speed set to level 3 (300–400 rpm). This process facilitated the dissolution of reactants and the formation of a homogeneous sol-gel solution with enhanced stability. Following this, the solution was transferred to an ultrasonic water bath (Hwasin Technology Powersonic 405, 40 kHz) and sonicated for 30 minutes at 50 °C. Sonication helped to break down larger agglomerates, ensuring particle size homogeneity and improved dispersion. The solution was then allowed to age at room temperature for an additional 30 minutes while being stirred at the same speed. After this process, the solution developed into a rich dark blue colour. Ethanolamine acted as a reducing agent, stabilizing the solution and preventing the formation of aggregates by chelating with copper (II) acetate via O–Cu–O and O–Cu–N bonds [22, 23]. The final solution was a clear, blue, particle-free sol, ready for spin coating. The spin coating process was carried out using two different spin durations (10 s and 30 s) and two spin speeds (1500 rpm and 3000 rpm). During the second stage of spin coating, 10 drops of the aged solution were applied. The coated samples were preheated at 100 °C for 10 minutes in ambient atmosphere to remove excess solvent. To achieve the desired film thickness, the deposition process was repeated to form a second layer, referred to as SL 2. Subsequently, all samples were annealed in a furnace at 300 °C for 1 hour to enhance crystallinity and improve film characteristics. After annealing, the glass substrates were allowed to cool for 10 minutes and were stored in a sealed, dry container. The samples were labelled as SL 1 (single-layer) and SL 2 (double-layer) films. Characterization of the films was conducted using X-ray diffraction (XRD; PANalytical X'Pert PRO), field emission scanning electron microscopy (FESEM; Apreo 2S, Thermo Fisher Scientific), and ultraviolet-visible-near infrared (UV-Vis-NIR) spectroscopy (Cary 5000). A schematic illustration of the CuO SL preparation process is shown in Figure 1.

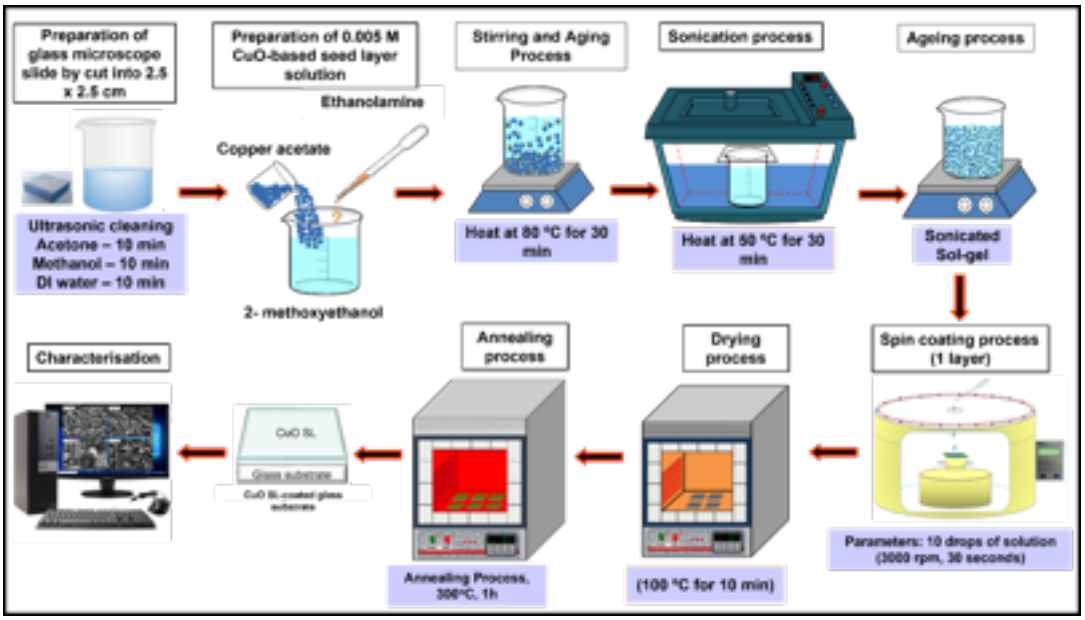

Fig. 1. Schematic diagram of CuO NPs seed layer prepared via ultrasonic-assisted sol-gel spin coating technique

2.2 Preparation of CuO nanostructures

In the subsequent stage, CuO Ns were deposited onto the previously prepared CuO NP SLs (SL 1 and SL 2). These SLs provided a stable foundation to promote uniform and oriented growth of the CuO Ns. To prepare the growth solution, 1000 mL of deionized (DI) water was measured and divided evenly among four 250 mL Schott bottles. An aqueous solution containing 20 mM copper(II) nitrate [$Cu(NO_3)_2$] as the precursor and 20 mM hexamethylenetetramine (HMTA) as the stabilizer was prepared. The required amounts of $Cu(NO_3)_2$ and HMTA were dissolved in DI water and stirred on a hotplate at 80 °C for 30 minutes at stirring speed level 3 (300–400 rpm), resulting in a clear, sky-blue solution. Following stirring, the solution was transferred to an ultrasonic water bath (Hwasin Technology Powersonic 405, 40 kHz) and sonicated at 50 °C for 30 minutes. Sonication facilitated the breakdown of agglomerates, ensuring uniform nanoparticle dispersion. The solution was then aged at room temperature for 1 hour to initiate nucleation and stabilize particle growth. Subsequently, it was stirred again at room temperature for an additional hour at the same speed (level 3) to ensure complete homogeneity prior to deposition. The aged solution was poured into 250 mL Schott bottles, and one CuO NP SL-coated FTO glass substrate was placed at the bottom of each bottle, with the coated side facing upward. Microwave-assisted growth was carried out using a SHARP 25 L microwave oven (Model R754AST). In this experiment, the microwave was operated at power levels P10 (≈100 W, 65-90 °C), P20 (≈200 W, 95-110 °C), and P30 (≈300 W, 110-150 °C). Notably, lower microwave powers were explored to improve energy efficiency and the functional properties of the nanostructures. The microwave power parameters and the seed layers used for CuO Ns growth are summarised in Table 1.

Table 1
The variable parameters with its level Microwave power growth

CuO NPs	CuO Ns	P10 (100 watt)	P20 (200 watt)	P30 (300 watt)
SL 1	Ns1	Ns1_P10	Ns1_P20	Ns1_P30
SL 2	Ns2	Ns2_P10	Ns2_P20	Ns2_P30

The reaction was allowed to proceed for 3 hours. This low-power condition was chosen to investigate the influence of reduced thermal input on CuO nanostructure growth and morphology. After completion, the substrates were removed from the solution and rinsed thoroughly under running DI water to eliminate residual precipitates. Following growth, the samples were dried and subsequently annealed in air at 300 °C for 1 hour to enhance crystallinity and remove any residual organic impurities. After annealing, samples were cooled to room temperature for 10 minutes and stored in a sealed, dry container. This step finalizes the fabrication of CuO Ns with well-defined morphological and structural characteristics. A schematic illustration of the CuO Ns formation process using the microwave-assisted sonochemical technique is shown in Figure 2.

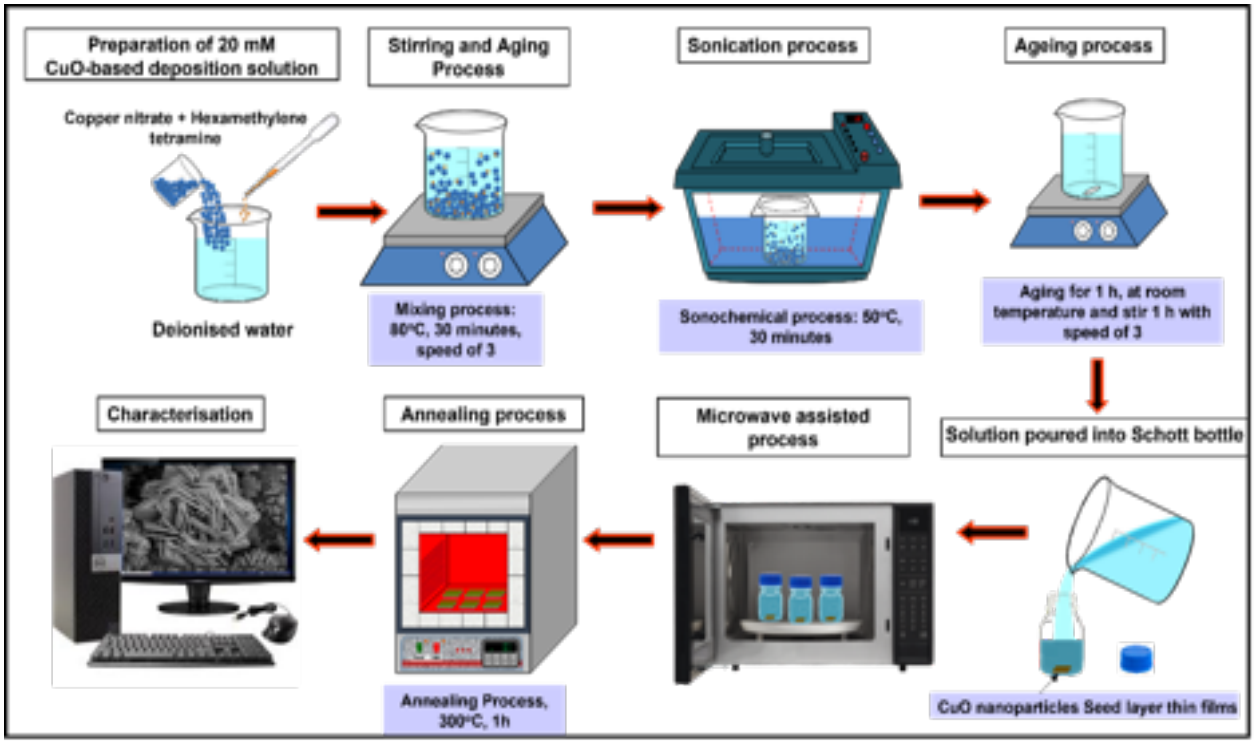

Fig. 2. Schematic diagram of CuO Ns thin film preparation via microwave assisted sonochemical technique.

2.3 Material characterisation

X-ray diffraction (XRD) was employed as a non-destructive technique to analyze the chemical composition and crystallographic structure of the CuO NSs, distinguishing between amorphous and crystalline phases. The measurements were performed using a PANalytical X'pert PRO XRD system with Cu Kα radiation (λ = 1.5406 Å) over a 2θ range of 30° to 80°, operating at 45 kV and 40 mA, with a scan rate of 2°/min. The surface morphology of the CuO NSs was examined using Field Emission Scanning Electron Microscopy (FESEM). Chemical composition was quantitatively analyzed by Energy Dispersive X-ray Spectroscopy (EDX), which offers energy resolutions of 161 eV for Cu Kα and 135 eV for Mn Kα lines. EDX spectra were used to identify and quantify elemental composition. Optical properties were measured using UV-Vis-NIR spectroscopy over a wavelength range of 200 to 1200 nm.

3. Result and Discussions

3.1 CuO seed layer thin film

3.1.1 Analysis of Field Emission Scanning Electron Microscopy (FESEM)

The surface morphology and size distribution of CuO nanoparticles (NPs) synthesized with varying numbers of SL are illustrated through FESEM images at low (30 kx) and high (100 kx) magnifications, as shown in Figure 3. To identify the optimal synthesis conditions, the effect of SL number on particle morphology, distribution, and film thickness was systematically investigated. The abundant presence of uniform nanoparticles in the images indicates that the synthesis method is effective and straightforward for producing CuO NPs. Figure 3(a) presents a top-view FESEM micrograph of CuO NPs deposited with a single seed layer (SL 1). The nanoparticles exhibit an asymmetric morphology composed of both small and large granules with varying sizes. The size distribution histogram in

Figure 3(b) shows an average particle size of approximately 38 nm for SL 1. Figure 3(c) shows FESEM images of CuO NPs synthesized with two seed layers (SL 2). The film morphology reveals a more uniform grain distribution on the FTO substrate, accompanied by an increase in film thickness. Correspondingly, the size distribution in Figure 3(d) indicates an average particle size of about 90 nm for SL 2. Consistent with Raad et al. [20], the shape and size of nanoparticles influence their magnetic properties, leading to variations in morphology. Moreover, it has been reported that CuO grain size correlates with film thickness, with grain size increasing as thickness increases [24].

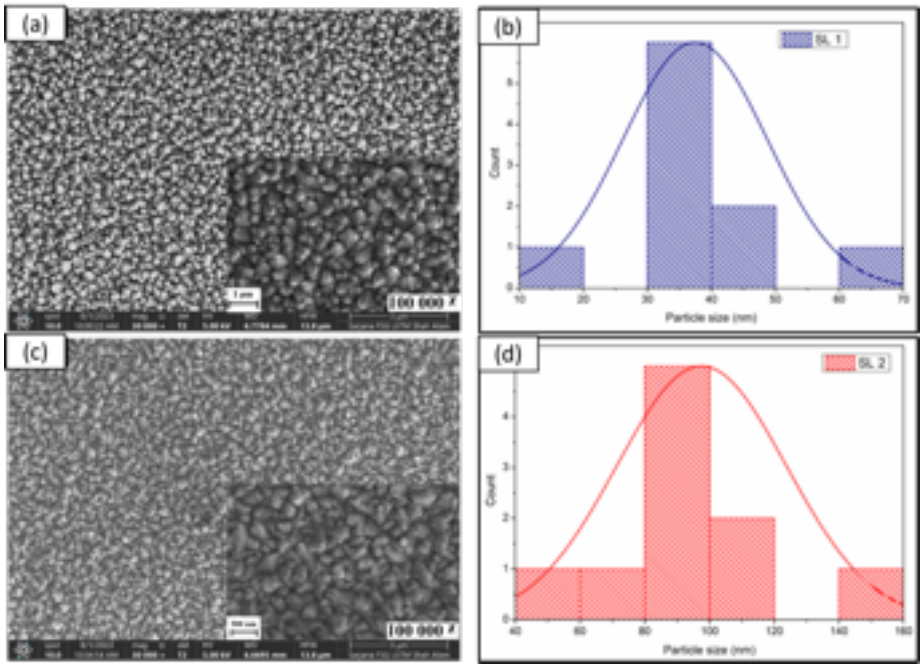

Fig. 3. a) FESEM images and b) size distribution of SL 1 CuO NPs; c) FESEM images and d) size distribution of SL 2 CuO NPs.

3.1.2 Analysis of X-ray Diffraction (XRD)

The structural properties of CuO nanoparticles (NPs) were investigated using X-ray diffraction (XRD) with Cu Kα radiation (λ = 0.154 nm). The CuO NPs were synthesized by a spin-coating method with varying numbers of seed layers (SL), ranging from one to two. The prepared samples exhibited a polycrystalline nature, as evidenced by the XRD patterns [25]. All diffraction peaks were indexed to the standard CuO diffraction patterns (ICSD card no. 01-089-2531). Figure 4 shows the typical XRD patterns of CuO NPs prepared with one and two seed layers. Peaks observed at approximately 34.30°, 38.37°, 52.04°, 62.22°, and 66.21° correspond to the (002), (111), (020), (-113), and (-313) crystallographic planes of monoclinic CuO, respectively. The peak intensities increased with the number of seed layers, indicating enhanced crystallinity. No impurity peaks were detected in the XRD patterns. Notably, the (111) peak was the most prominent, with additional minor peaks corresponding to the (002), (020), (-113), and (-311) planes observed in the CuO thin films. This preferential orientation along the (111) plane is attributed to its lower surface energy [13].

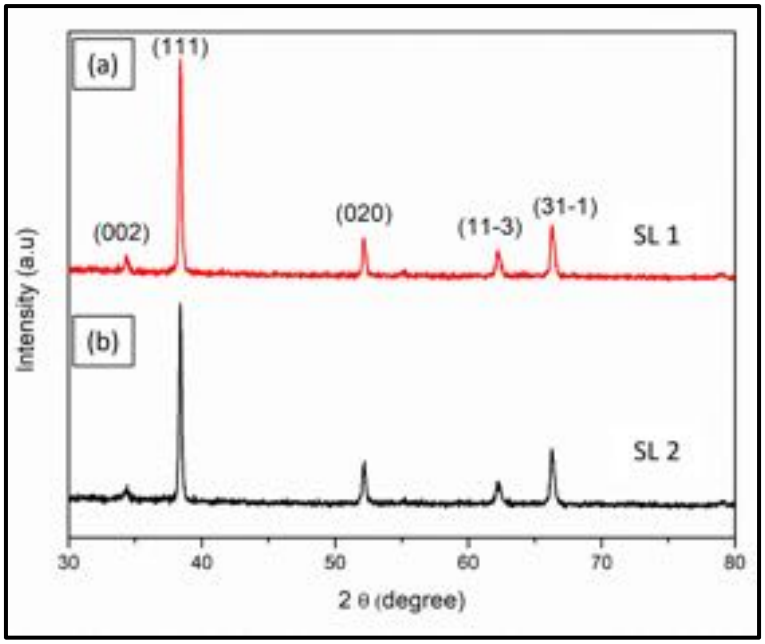

Fig. 4. The XRD spectra of CuO NPs at different number of layers (a) SL 1 and (b) SL 2.

3.1.3 Analysis of UV-Vis NIR Spectroscopy

The optical transmittance spectra of copper oxide (CuO) thin films were measured using a UV-Vis spectrophotometer. Figure 5 presents the transmittance spectra recorded over the wavelength range of 300 nm to 1200 nm for CuO thin films prepared with different numbers of seed layers (SL). The film fabricated with a single seed layer (SL 1) exhibited a maximum transmittance of 88% in the visible region. However, increasing the number of seed layers from one to two resulted in a decrease in transmittance from 88% to 63%. This reduction in optical transmittance can be attributed to the increased film thickness associated with the additional seed layer. Thicker films generally absorb and scatter more incident light due to a larger volume of active material and increased surface roughness, leading to enhanced light attenuation. Consequently, the observed decrease in transmittance is consistent with the expected optical behavior of multilayered or thickened CuO films, where greater light–matter interactions occur within the film structure. Additionally, the CuO films with two seed layers (SL 2) showed relatively strong absorption in the 300 nm to 900 nm wavelength range, with lower absorbance in the infrared and near-infrared regions [12].

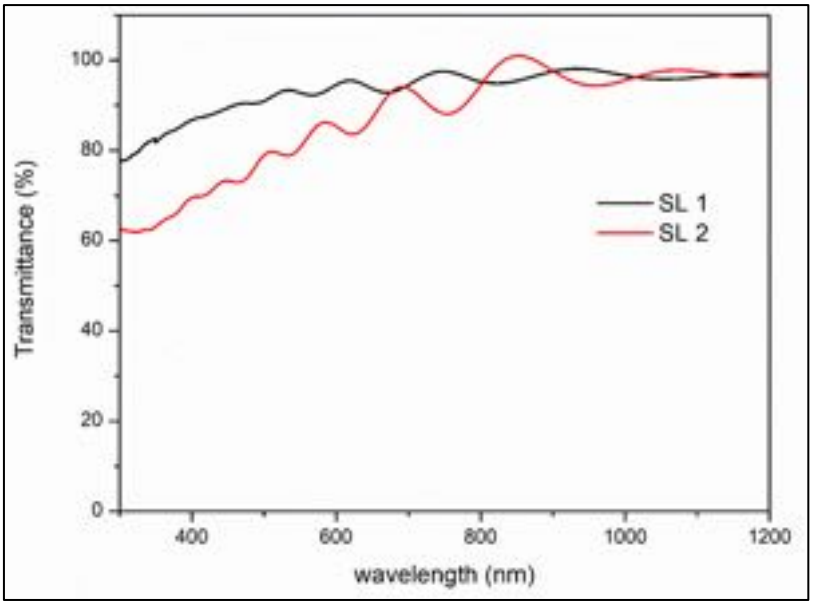

Fig. 5. Transmittance spectra of CuO NPs with different number of layers.

3.2 The growth of CuO Nanostructures

3.2.1 Analysis of Field Emission Scanning Electron Microscopy (FESEM)

Figure 6 presents the field emission scanning electron microscopy (FESEM) images of the surface morphology of CuO Ns at 30kx magnification, along with the corresponding size distributions of the CuO thin films. The CuO Ns were uniformly distributed over the FTO substrates, consisting of randomly shaped, densely packed particles with minimal interparticle spacing, as observed in the FESEM images of the Ns1 samples. Similar agglomerated formations of CuO Ns synthesized via ultrasonic spray pyrolysis have been reported by Muhammed et al. [14]. In Figure 6(a), the Ns1_P10 sample exhibits semi-spherical grains with some surface irregularities, resulting in a rough, granular texture. No petal-like structures are observed, indicating incomplete film formation. The size distribution of CuO Ns in the Ns1_P10 sample, characterized by agglomerated nanostructures, ranges from 200 nm to 550 nm, with an average size of approximately 367 nm.

In contrast, the Ns1_P20 sample shown in Figure 6(b) displays densely packed, leaf- and flower-like structures, forming a textured and homogeneous layer. These structures are closely aligned and uniform, suggesting consistent nucleation and growth across the film surface. Figure 6(c), depicting the Ns1_P30 sample, reveals larger plate-like structures embedded within a matrix of smaller sheet-like particles. The coexistence of sheet- and pyramid-like structures suggests hierarchical growth, likely influenced by nucleation sites associated with the seed layers. Figures 6(d), (e), and (f) show FESEM images of CuO Ns thin films deposited with two seed layers (Ns2). The overall morphology of samples Ns2_P20 and Ns2_P30 is characterized by triangular-shaped petal-like structures, which assemble into flower-like formations composed of two-dimensional (2D) nanosheets clustered locally.

However, the relatively sparse flower-shaped nanostructures in Figure 6(d) indicate that the flower clusters, composed of multiple triangular petals, are less uniformly distributed compared to Ns1_P10. The morphology of Ns2_P20 (Figure 6(e)) reveals a dense network of elongated, sheet-like particles exhibiting greater size variability than Ns1_P10. Meanwhile, Ns2_P30 (Figure 6(f)) displays a less uniform surface with regions of agglomeration, likely reflecting differences in deposition power. Overall, these observations suggest that CuO Ns grown with a single seed layer (Ns1) promote

more uniform and consistent film growth, whereas films with two seed layers (Ns2) exhibit less uniformity and a wider variety of morphologies. This variability may result from differences in film thickness, composition, or other growth parameters. Additionally, the observed structures are consistent with a monoclinic crystal phase of CuO [26]. According to the Bravais-Donnay-Harker Law [27], the crystal growth rate is typically proportional to 1/dhkl. $Cu(OH)_2$ preferentially grows along the (111) crystallographic plane, promoting the formation of one-dimensional (1D) fibril-like and three-dimensional (3D) flower-like nanostructures.

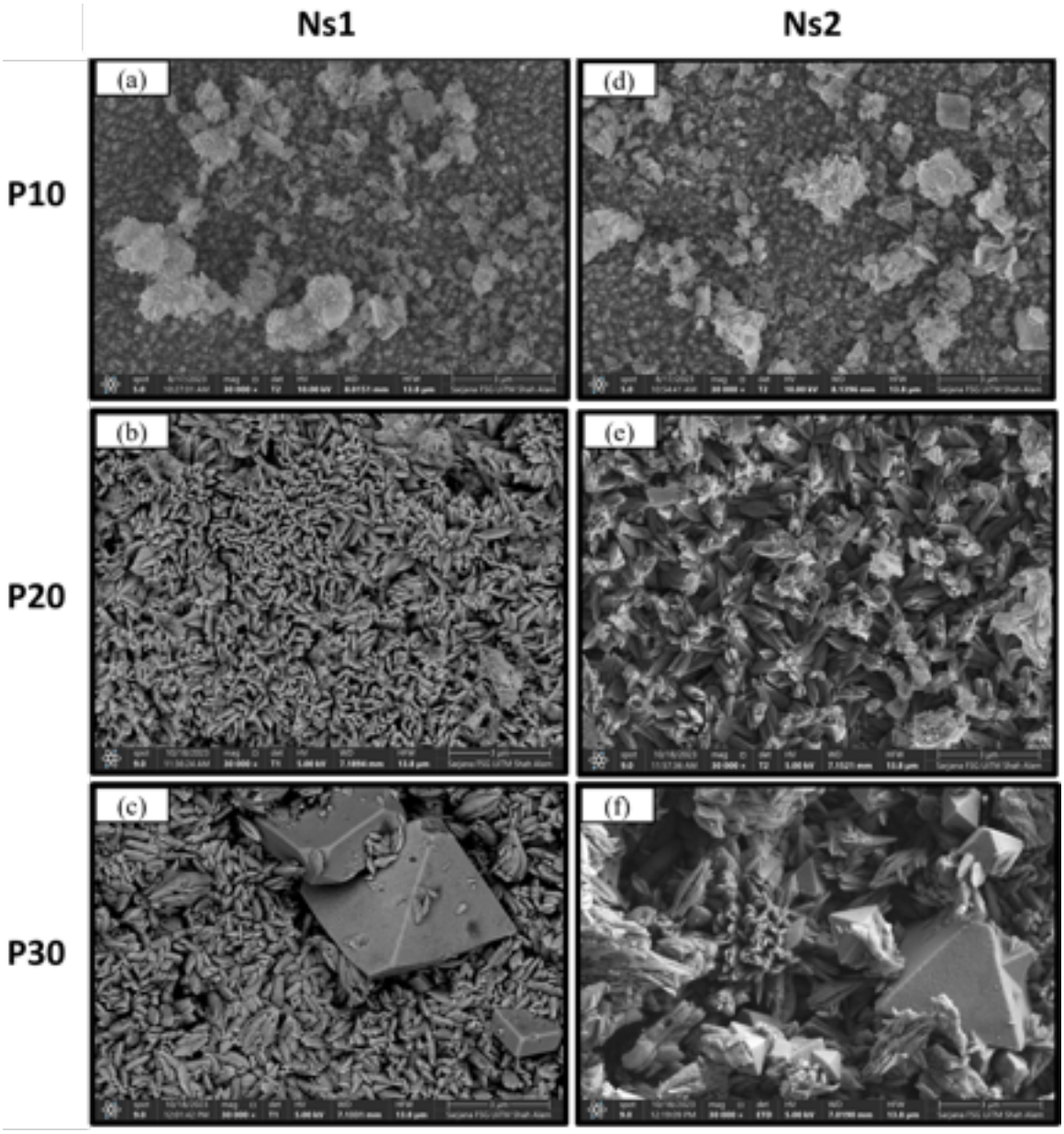

Fig. 6. Surface FESEM images of CuO NS thin film at low magnification (30kx) prepared at various microwave power (a) Ns1_P10 (b) Ns1_P20 (c) Ns1_P30 (d) Ns2_P10 (e) Ns2_P20 and (f) Ns2_P30

Due to the strong ability of hexamethylenetetramine (HMTA) to coordinate with Cu^{2+} ions, the addition of HMTA during the microwave-assisted sonochemical synthesis of CuO nanostructures (Ns) can alter the structure-directing mechanism. Upon the introduction of HMTA, a sky-blue precipitate immediately forms, which slows the growth of certain crystallographic planes and promotes the

formation of nanosheets [28]. Although the formation mechanisms of flower- and sheet-like CuO nanostructures have been discussed, further investigations are necessary to provide more definitive evidence of their growth processes.

3.2.2 Analysis of Energy Dispersive X-Ray Spectroscopy (EDX)

Figure 7 shows the EDX spectra of the CuO thin films, while the composition of copper (Cu) and oxygen (O) is summarized in the accompanying table. It is worth noting that the EDX analysis was performed on the surface of the samples at a magnification of 30 kx. For both Ns1 and Ns2, Cu and O are the dominant elements, confirming the presence of CuO Ns in the samples. The minor carbon (C) content may result from contamination or the underlying substrate material. Notably, the power level used during synthesis and the substrate layer (SL) influenced the percentage of Cu atoms. The highest copper percentage was observed in the Ns1_P20 sample, with 58.65 wt.% compared to 56.93 wt.% in the Ns2_P20 sample, as shown in Figures 7(b) and 7(e). The high content of Cu and O validates that the observed nanostructures could be nanoflowers, nanosheets, or nanoleaves of CuO. In contrast, lower Cu content was observed at the lowest power level (P10), indicating that the thin film Ns may contain less CuO [29]. This lower copper content at P10 can be attributed to insufficient thermal energy to fully decompose the precursor during synthesis.

Therefore, microwave power in the microwave-assisted method can be considered analogous to temperature in conventional hydrothermal systems, with both requiring optimization to achieve uniform CuO Ns with high crystallinity. At higher microwave power levels for SL1 (Ns1), shown in Figures 7(b) and 7(c), copper concentrations were 58.65% and 54.19%, respectively. In contrast, samples prepared under lower power (P10), shown in Figures 7(a) and 7(d), exhibited significantly lower copper content of only 8.04% and 4.66%, respectively. A similar trend was observed for the Ns2 samples from the SL2 group, with Cu content of 56.93% and 51.87% in Figures 7(e) and 7(f), respectively.

A comparison of these measurements suggests that the weight percentages of Cu and O elements are related to the penetration of Cu microcrystals originating from the $Cu(CH_3COO)_2$ and $CuNO_3$ precursors. The EDX results demonstrate improved CuO nanostructure quality with optimized microwave power. These findings imply that optimal microwave power enhances the breakdown of Cu precursors, which in turn promotes the penetration and incorporation of Cu^{2+} ions into the film. Overall, the EDX analysis confirms that microwave power is a critical parameter in the synthesis of high-quality CuO Ns, as it directly influences Cu diffusion and film composition. Conversely, lower microwave power levels, such as P10, generate insufficient thermal energy, leading to incomplete precursor decomposition and reduced Cu diffusion. These conclusions are supported by the EDX results, which show improved CuO nanostructure quality and Cu content with optimized microwave power.

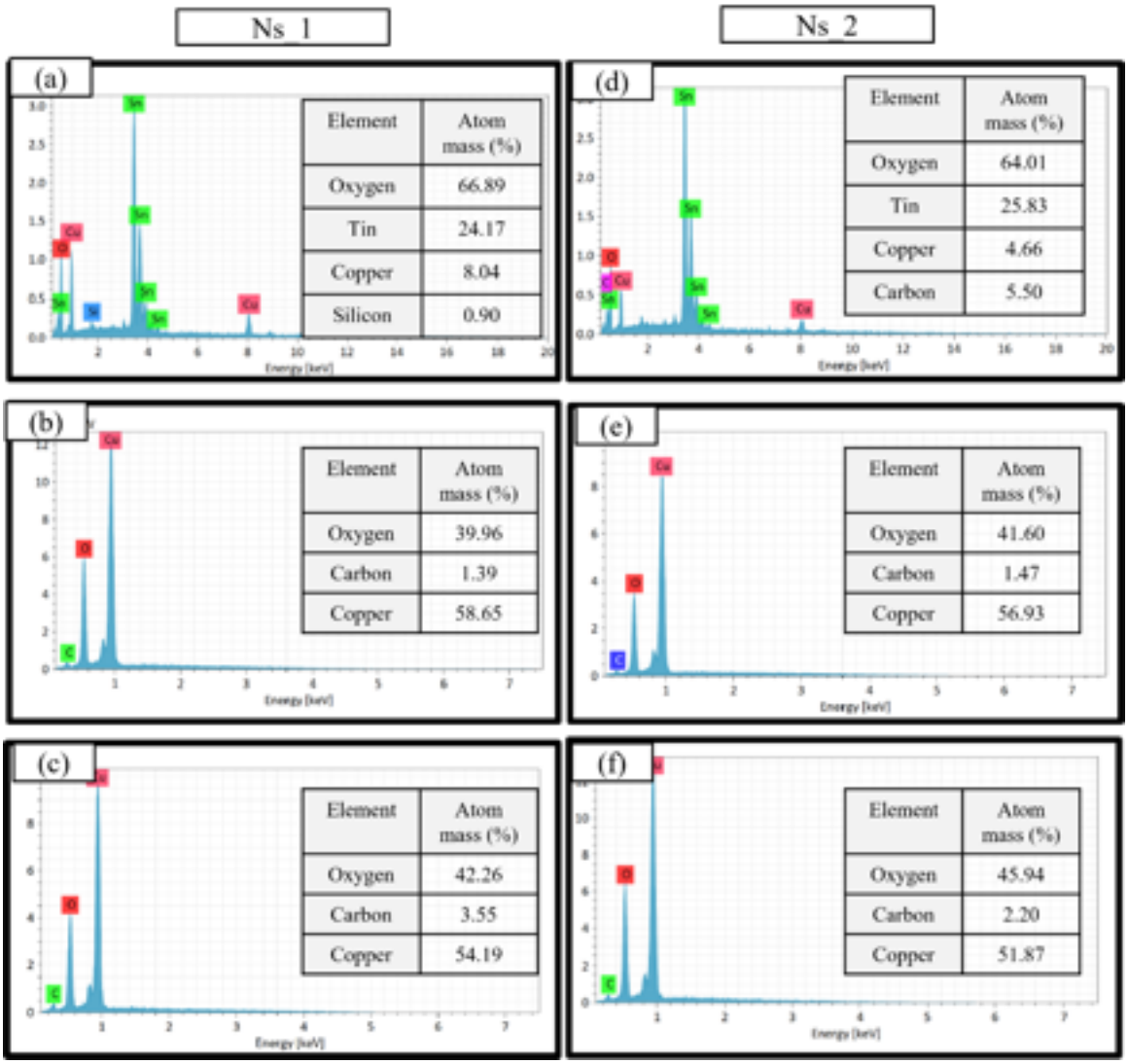

Fig. 7. EDX analysis of CuO Ns prepared at various microwave power (a) Ns1_P10 (b) Ns1_P20 (c) Ns1_P30 (d) Ns2_P10 (e) Ns2_P20 and (f) Ns2_P30

Figure 8 illustrates the morphological evolution of the films from triangular-shaped petal structures to flower-like formations composed of 2D nanosheets. As the microwave power increased from P10 to P20, the nanosheets exhibited improved uniformity and packing density. Samples Ns1_P20 and Ns2_P20, shown in Figures 8(b) and 8(e), formed hierarchical architectures characterized by rough, compact surfaces and well-distributed particle arrangements, which are favorable for enhancing crystallinity and light absorption. Additionally, Ns1_P20 and Ns2_P20 produced smaller and more consistent particle sizes, ranging from 341 to 391 nm.

These results confirm that microwave power significantly influences particle morphology, with P20 identified as the optimal condition for synthesizing well-defined CuO nanostructures. In contrast, at higher power (P30), the films exhibited larger, flower-like structures with reduced uniformity, particularly in Ns2_P30 (Figure 8(f)), which displayed the largest average particle size of approximately 860 nm. Ns1_P30 also showed increased particle size, averaging about 680 nm, whereas both Ns1_P20 and Ns2_P20 maintained smaller, more uniform particle sizes within the 341–391 nm range. Table 2 summarises the particle sizes corresponding to varying microwave power levels under different SL for the CuO thin films.

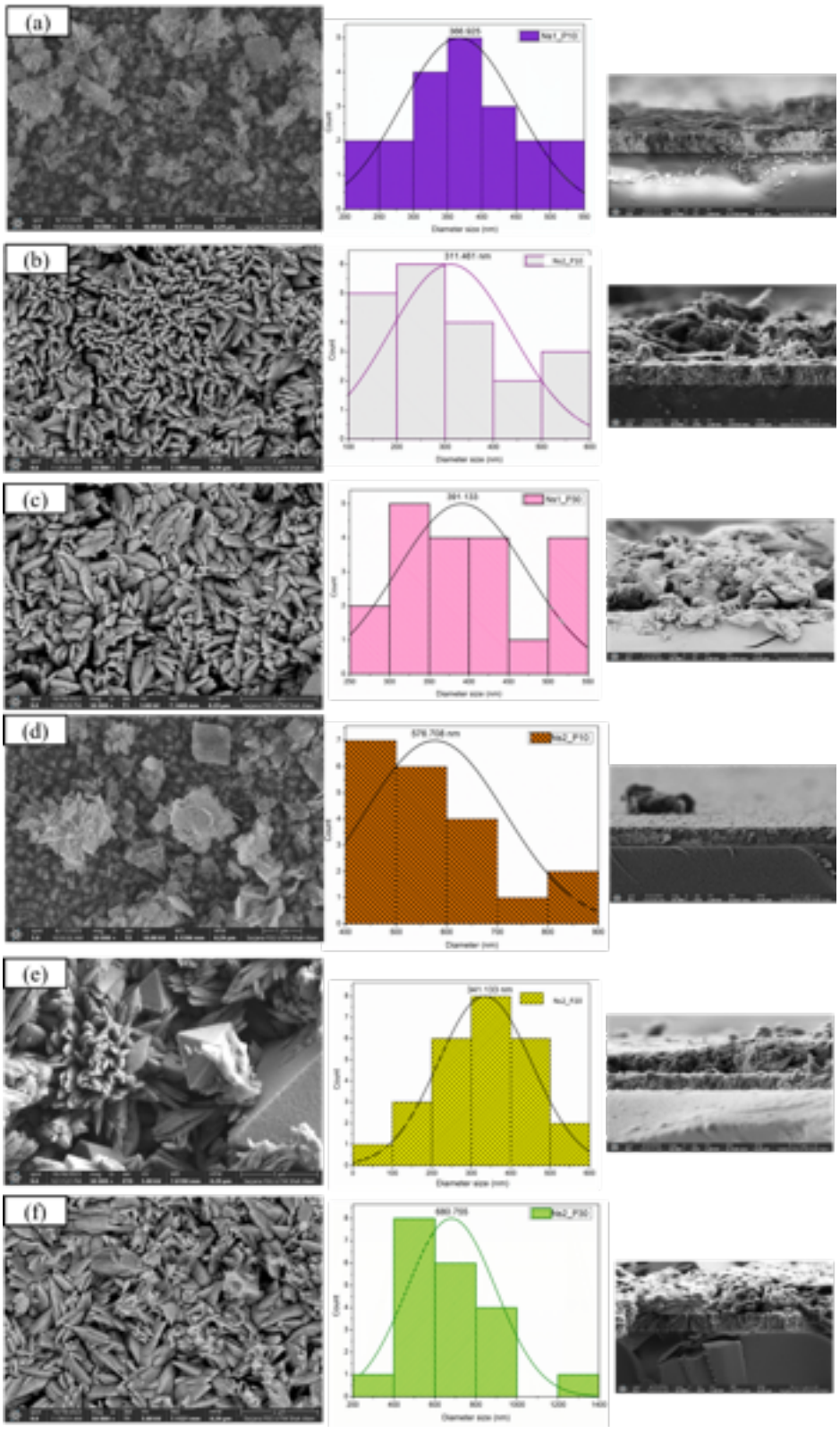

Fig. 8. Surface morphology, cross-section and size distribution of CuO Ns thin film at 50 kx magnification prepared at various microwave power (a) Ns1_P10 (b) Ns1_P20 (c) Ns1_P30 (d) Ns2_P10 (e) Ns2_P20 and (f) Ns2_P30

These CuO nanoflakes, nanosheets, and nanoflowers exhibit unique p-type semiconductor properties, including a large surface area and enhanced light absorption. Due to their increased surface area and improved light-trapping capabilities, hierarchical structures especially flower-like morphologies are advantageous for applications such as photocatalysis, solar energy harvesting, and gas sensing. The diversity in CuO nanostructures, ranging from nanoflakes to flower-like forms, highlights the significant influence of SL and processing conditions on the resulting film characteristics.

Table 2
The average results thickness and estimated particle size distribution of CuO Ns thin film prepared at various microwave power.

Samples	No. of seed layer	Temperature range of microwave (Based on Sharp model) (°C)	Time of growth (H)	Average Results Thickness (µm)	Estimated Particle size (nm)
Ns1_P10	1	65-90	3	2.807	366.925
Ns1_P20	1	90-110	3	3.263	311.461
Ns1_P30	1	110-150	3	7.847	391.133
Ns2_P 10	2	65-90	3	0.744	576.708
Ns2_P20	2	90-110	3	2.529	341.133
Ns2_P30	2	110-150	3	2.823	680.755

3.2.3 Analysis of X-ray Diffraction (XRD)

Figure 9 presents the XRD patterns of CuO nanostructure (Ns) samples synthesized with different numbers of substrate layers (SL). The diffraction peaks observed at 2θ = 35.5°, 38.5°, 53.5°, 61.5°, and 68.1° correspond to the (002), (111), (020), (1$\bar{1}$3), and (3$\bar{1}$1) crystal planes, respectively, characteristic of the monoclinic CuO phase (ICSD Card No. 01-089-2531) with lattice parameters a = 4.6691 Å, b = 3.4805 Å, c = 5.1183 Å, and β = 98.595°, consistent with previously reported results [1]. No characteristic peaks of impurities were detected, except for minor traces of copper. Among all six CuO Ns samples, the (111) peak was the most prominent. The monoclinic structure of CuO is evident in all XRD spectra, reflecting the crystallographic nature of CuO. This phenomenon is closely related to the growth mechanism of CuO nanostructures during deposition, which is significantly influenced by the number of substrate layers.

There is a direct relationship between peak broadening at specific 2θ angles and crystallite size: broader peaks correspond to smaller crystallite sizes [1]. The study revealed that the crystallite size of CuO decreased when the synthesis was performed from SL1 to SL2 [3]. Specifically, CuO Ns synthesized on seed layer 1 (Ns1) exhibited well-defined, broad crystalline peaks compared to those synthesized on seed layer 2 (Ns2). The increased density of nucleation centers in Ns2 inhibits crystal grain growth, leading to a reduction in crystallite size [13]. This suggests that the SL2 substrate layer likely promotes additional nucleation sites, which can alter crystal growth, texture, and morphology. These modifications may explain the observed variations in peak intensities and sharpness across samples. The crystallite size was calculated by analyzing the width of the diffraction peaks using Scherrer's formula [30]. The application of Scherrer's formula to the CuO Ns thin films yielded the following equation Eq. (1):

$$D = \frac{K\lambda}{\beta \cos\theta} \quad (1)$$

where, D represents the crystallite size in nanometers (nm). The constant K is assigned a value of 0.94, representing the shape factor. The wavelength of the X-ray source, λ, is 0.15406 nm. The parameter β denotes the full width at half maximum (FWHM) of the broadened diffraction peak on the 2θ scale, measured in radians. θ corresponds to the Bragg angle, which is half of the diffraction angle 2θ, expressed in radians. The structural parameters, including the crystallite size of the CuO nanostructures (Ns), are summarized in Table 3. From the XRD analysis, it was observed that the Ns2 group, corresponding to a higher number of substrate layers (SL), exhibited larger crystallite sizes. This suggests that the crystallite size of CuO Ns thin films is influenced by both the number of SLs and the optimization of microwave power.

Specifically, increasing both the number of SLs and the microwave power resulted in larger crystallite sizes. The relatively smaller crystallite size observed in Ns1_P10 can be attributed to a combination of factors, including a high nucleation density, non-uniform surface morphology, and limited atomic mobility at lower microwave power. Among all samples, Ns1_P20 displayed a well-balanced crystallite size of 35.57 nm, accompanied by well-defined broad peaks, indicating high crystallinity while maintaining fine nanostructure features. This is further supported by FESEM images, which show that Ns1_P20 possesses a uniform distribution of small, well-defined nanostructures with homogeneous grain distribution, making it the optimal sample in this study. Such uniformity in particle size and morphology is critical for applications demanding enhanced optical and electrical properties. Conversely, Ns2_P30 exhibited larger and less uniform structures, which could negatively impact performance consistency.

In the Ns1 samples, the number of nucleation sites is lower compared to Ns2, providing more space for individual crystal grains to grow larger before impinging upon neighboring grains, resulting in increased crystallite size. Higher microwave power (P30) supplies greater energy, enhancing atomic mobility and grain growth. This increased energy can facilitate the coalescence of smaller crystallites into larger ones, thereby increasing the average crystallite size. Moreover, the lower nucleation density in Ns1_P30 reduces internal stress and strain, enabling easier crystal expansion and growth [30]. The crystallinity and optical behavior of the CuO Ns synthesized here were compared with previous literature to evaluate relative improvements. All samples demonstrated the monoclinic CuO phase with pronounced diffraction peaks, particularly along the (111) plane, indicating strong crystallinity. The observed smaller FWHM values and enhanced peak intensities further confirm improved crystalline quality, consistent with the findings reported by Özmenteş [18].

Table 3
Structural parameters of the CuO Ns thin film prepared at various microwave power

Plane	Samples	Peak position (°)	FWHM (°)	Crystallite Size (nm)	Phase
(111)	Ns1_P10	38.361	0.004695	32.65 nm	monoclinic
	Ns1_P20	38.493	0.004311	35.57 nm	monoclinic
	Ns1_P30	38.353	0.003927	39.03 nm	monoclinic
	Ns2_P 10	38.365	0.003962	38.69 nm	monoclinic
	Ns2_P20	38.417	0.004276	35.85 nm	monoclinic
	Ns2_P30	38.364	0.004224	36.29 nm	monoclinic

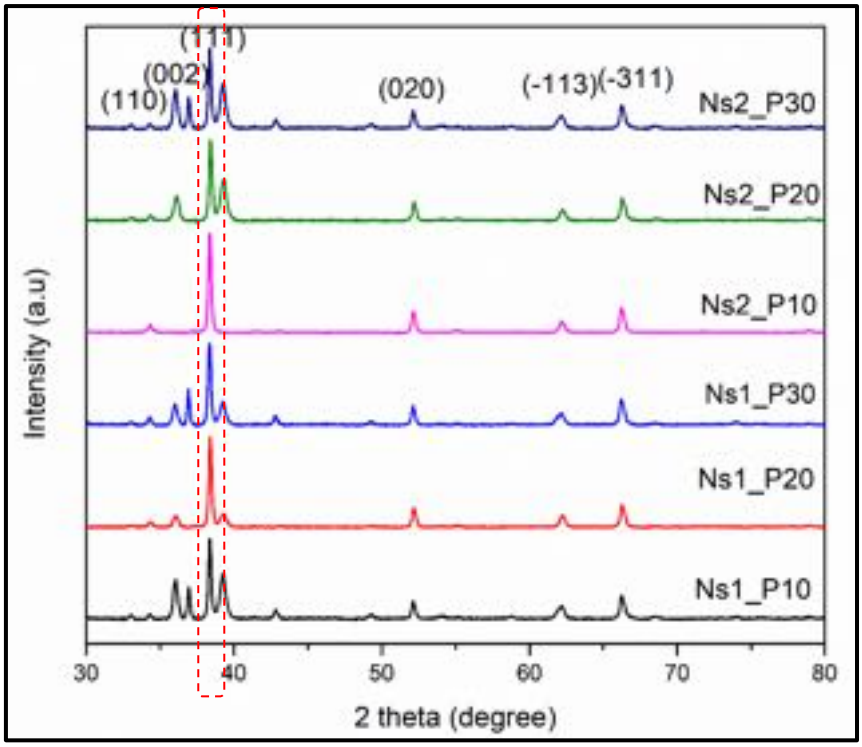

Fig. 9. The XRD pattern of CuO Ns thin film prepared at various microwave power

3.2.4 Analysis of UV-Vis NIR Spectroscopy

Additionally, the transmittance of the CuO thin films was measured using a UV–Vis spectrometer, as shown in Figure 10. Among the samples, the Ns1 group exhibited the highest average transmittance within the visible wavelength range, which was sensitive to the film thickness. From the transmittance spectra, the sample synthesized at P20 demonstrated optimal properties, characterized by lower transmittance. This decrease in transparency with increasing film thickness was expected, as thicker films absorb more photons. Furthermore, as the film thickness increased, the crystalline grain structures likely became denser, as evidenced by the FE-SEM images, which reduced the ease with which light could pass through the film surface. In agreement with this, the optical transmittance of the films decreased with increasing film thickness and microwave power. The best-performing sample, Ns1_P20, exhibited a well-balanced optical profile, combining moderate transmittance with strong absorption in the visible region. This performance surpasses the irregular or weak optical absorption reported in previous studies using sol-gel or hydrothermal synthesis methods [24]. These improvements can be attributed to the homogeneous morphology and controlled grain growth achieved through the microwave-assisted synthesis process.

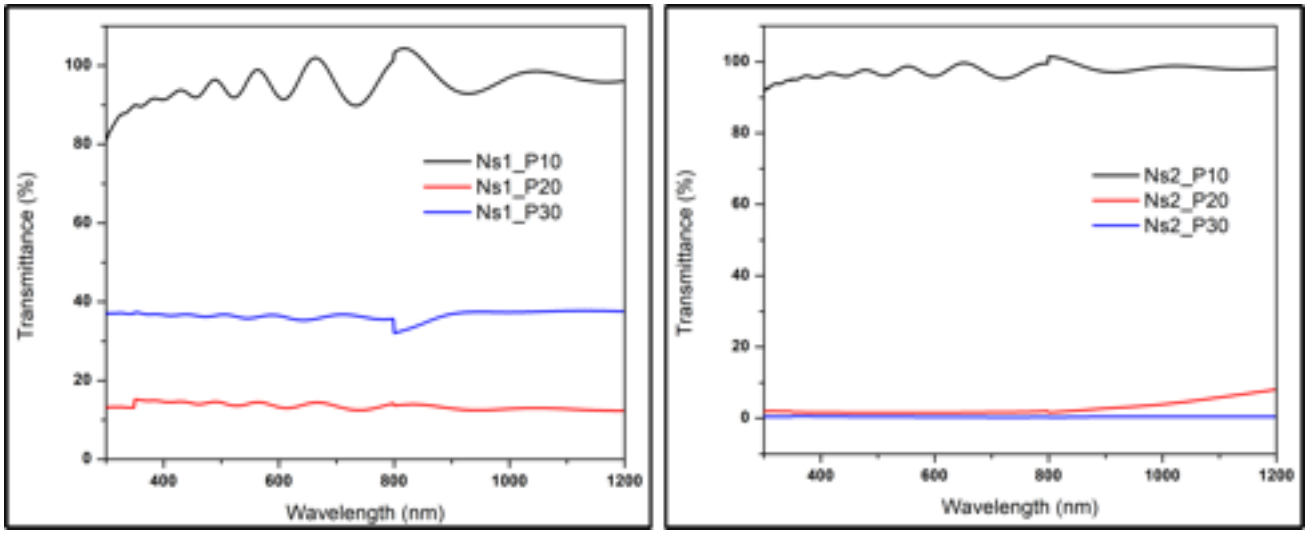

Fig. 10. Transmittance spectra of CuO Ns with different number of seed layers and microwave powers

4. Conclusion

This study investigated the synthesis of CuO nanostructured thin films on FTO substrates using a microwave-assisted sonochemical method. The results confirmed the successful deposition of CuO nanostructures, with their morphological and structural properties strongly influenced by both the number of SL and the applied microwave power. FESEM analysis revealed that a single seed layer (Ns1) produced more uniform and well-defined CuO nanopetals, whereas two seed layers (Ns2) promoted the formation of more complex morphologies, including nanosheets, nanopyramids, and nanoflowers, alongside increased film thickness and greater morphological variation. Among the microwave power levels tested (P10, P20, and P30), P20 was identified as the optimal power setting, yielding compact, uniform, and well-distributed CuO nanostructures with enhanced crystallinity and improved light absorption. XRD analysis confirmed that all films were polycrystalline with a monoclinic CuO phase, exhibiting a preferential orientation along the (111) plane. Optical measurements indicated that films with greater thickness exhibited lower transmittance, further validating the impact of SL number and microwave power on film density and optical performance. In summary, the optimal conditions for producing high-quality CuO thin films were determined to be a single seed layer combined with microwave power at P20. This approach not only simplifies the synthesis process but also reduces the time required for film formation and characterization, making it a promising method for scalable and efficient production of CuO-based thin films for light absorption applications in solar cells.

Acknowledgement

This work was supported by grant no. 600-RMC/GIP 5/3 (065/2023). The authors would like to thank the Research Management Centre (RMC), Universiti Teknologi MARA (UiTM), Malaysia for their support. The authors also thank Mr. Salifairus Mohammad Jafar (UiTM Senior Science Officer), Mr. Mohd Azlan Jaafar (UiTM senior assistant engineer) and Mr. Muhamad Faizal Abd Halim (Assistant Research Officer) for their kind support on this research.

References

[1] Ahmad Z Al-Jenaby, Abdul-Majeed E Al-Samarai, and Asmiet Ramizy. "Effect of reaction time on the physical properties of CuO/PS nanostructures prepared via the hydrothermal method." *Materials Today: Proceedings* 42 (2021): 2840-2844. https://doi.org/10.1016/j.matpr.2020.12.731

[2] Youngjae Kim, JaeDong Lee. "Time-resolved photoemission of infinitely periodic atomic arrangements: correlation-dressed excited states of solids." *npj Computational Materials* 6, no. 1 (2020): 132. http://dx.doi.org/10.1038/s41524-020-00398-0

[3] Mohammad Yeganeh GhotbiZahra Rahmati. "Nanostructured copper and copper oxide thin films fabricated by hydrothermal treatment of copper hydroxide nitrate." *Materials & Design* 85 (2015): 719-723 DOI: https://doi.org/10.1016/j.matdes.2015.07.081.

[4] H Hashim, SS Shariffudin, MSP Sarah, and NI Nasir. *The characterization of copper oxide with different molar concentration using sol-gel spin coating*. in *2016 IEEE International Conference on Semiconductor Electronics (ICSE)*. 2016. IEEE. http://dx.doi.org/10.1109/SMELEC.2016.7573632

[5] A MainiMA Shah. "Sol-Gel Fabricated CuO Thin Film: Characterization for Device Application." (2021). http://dx.doi.org/10.21272/jnep.13(5).05018

[6] Esraa Ahmed Mohammed. "Effect of Annealing on Sensing Properties of ZnO: CuO Nanocomposite Thin Films by the Sol-gel Method." *NeuroQuantology* 20, no. 2 (2022): 32. http://dx.doi.org/10.14704/nq.2022.20.2.NQ22021

[7] A. Bhaumik, A. Haque, P. Karnati, M. F. N. Taufique, R. Patel, and K. Ghosh. "Copper oxide based nanostructures for improved solar cell efficiency." *Thin Solid Films* 572 (2014): 126-133 DOI: https://doi.org/10.1016/j.tsf.2014.09.056.

[8] Shivaji B. Sadale, Sushant B. Patil, Aviraj M. Teli, Hikaru Masegi, and Kei Noda. "Effect of deposition potential and annealing on performance of electrodeposited copper oxide thin films for supercapacitor application." *Solid State Sciences* 123 (2022): 106780 DOI: https://doi.org/10.1016/j.solidstatesciences.2021.106780.

[9] Md Abdul Majed Patwary, Md Alauddin Hossain, Bijoy Chandra Ghos, Joy Chakrabarty, Syed Ragibul Haque, Sharmin Akther Rupa, Jamal Uddin, and Tooru Tanaka. "Copper oxide nanostructured thin films processed by SILAR for optoelectronic applications." *RSC advances* 12, no. 51 (2022): 32853-32884. https://doi.org/10.1039/d2ra06303d

[10] Hossain M. Zabed, Jahidul Islam, Faisal I. Chowdhury, Mei Zhao, Mukesh Kumar Awasthi, Abdul-Sattar Nizami, Jamal Uddin, Sabu Thomas, and Xianghui Qi. "Recent insights into heterometal-doped copper oxide nanostructure-based catalysts for renewable energy conversion and generation." *Renewable and Sustainable Energy Reviews* 168 (2022): 112887 DOI: https://doi.org/10.1016/j.rser.2022.112887.

[11] Amany Khaled, Nahed El-Mahallawy, Madiha Shoeib, and RA Atia. "DESIGN OF SOL-GEL COPPER OXIDE BASED COATING FOR SOLAR ENERGY APPLICATIONS." *Journal of Al-Azhar University Engineering Sector* 14, no. 50 (2019): 245-257. https://doi.org/10.21608/AUEJ.2019.28513

[12] Mehdi Dhaouadi, Mohamed Jlassi, Imen Sta, I Ben Miled, George Mousdis, Michael Kompitsas, and Wissem Dimassi. "Physical properties of copper oxide thin films prepared by sol–gel spin–coating method." *Am. J. Phys. Appl* 6, no. 2 (2018): 43-50. https://doi.org/10.11648/j.ajpa.20180602.13

[13] D Naveena, R Dhanabal, and A Chandra Bose. "Investigating the effect of La doped CuO thin film as absorber material for solar cell application." *Optical Materials* 127 (2022): 112266. https://doi.org/10.1016/j.optmat.2022.112266

[14] Muhammed Emin Güldüren, Demet İskenderoğlu, Harun Güney, Emre Gür, Merve Acar, and Sibel Morkoç Karadeniz. "Investigating the influence of Ni doping on the CuO thin films deposited via ultrasonic spray pyrolysis: Structural, optical and H2 gas sensing analyses." *International Journal of Hydrogen Energy* 48, no. 2 (2023): 828-839. https://doi.org/10.1016/j.ijhydene.2022.09.283

[15] Priyanka Marathey, Sakshum Khanna, Sagar Paneliya, and Anjali Vanpariya. "Fabrication of copper oxide nanostructures for visible-light photodetector." *Materials Today: Proceedings* 50 (2022): 129-133 DOI: https://doi.org/10.1016/j.matpr.2021.08.115.

[16] Farhan Arshad, Akhtar Munir, Qasim Qayyum Kashif, Tanveer ul Haq, Javed Iqbal, Falak Sher, and Irshad Hussain. "Controlled development of higher-dimensional nanostructured copper oxide thin films as binder free electrocatalysts for oxygen evolution reaction." *International Journal of Hydrogen Energy* 45, no. 33 (2020): 16583-16590. https://doi.org/10.1016/j.ijhydene.2020.04.152

[17] Ravi Kumar CheedaralaJung Il Song. "Face-centred cubic CuO nanocrystals for enhanced pool-boiling critical heat flux and higher thermal conductivities." *International Journal of Heat and Mass Transfer* 162 (2020): 120391. http://dx.doi.org/10.1016/j.ijheatmasstransfer.2020.120391

[18] Reşit ÖZMENTEŞ. "Effect of thermal annealing time on the optical characteristics of CuO thin films." *Yüzüncü Yıl Üniversitesi Fen Bilimleri Enstitüsü Dergisi* 24, no. 3 (2019): 176-182.

[19] Robert Mroczyński, Monika Ożga, Marek Godlewski, and Bartłomiej S Witkowski. "Hydrothermally formed copper oxide (CuO) thin films for resistive switching memory devices." *Solid-State Electronics* 194 (2022): 108357. https://doi.org/10.1016/j.sse.2022.108357

[20] Raad Q Abdalamir, Ziad T Khodair, and Ahmed N Abd. "Preparation and characterization of structural properties for TiO2 and CuO nanostructures by sol-gel technique." *Materials Today: Proceedings* 57 (2022): 539-544. https://doi.org/10.1016/j.matpr.2022.01.417

[21] Soroosh Mahmoodi, Dhia A Hassan, Akbar Hojjati-Najafabadi, Wei Li, Liefa Liao, Ata Jahangir Moshayedi, Xueyu Huang, and Mehrdad Nouri Khajavi. "Quality enhancement of copper oxide thin film synthesized under elevated gravity acceleration by two-axis spin coating." *Ceramics International* 46, no. 6 (2020): 7421-7429. . https://doi.org/10.1016/j.ceramint.2019.11.238

[22] Nitumoni Deka, Pinak Chakraborty, Dulal Chandra Patra, and Suvra Prakash Mondal. "Highly conducting flake-like CuS nanostructured counter electrode for photoelectrochemical solar energy conversion." *Thin Solid Films* 774 (2023): 139847. https://doi.org/10.1016/j.tsf.2023.139847

[23] Yee-Fun Lim, Chin Sheng Chua, Coryl Jing Jun Lee, and Dongzhi Chi. "Sol–gel deposited Cu 2 O and CuO thin films for photocatalytic water splitting." *Physical Chemistry Chemical Physics* 16, no. 47 (2014): 25928-25934. http://dx.doi.org/10.1039/C4CP03241A

[24] SS Shariffudin, SS Khalid, NM Sahat, MSP Sarah, and H Hashim. *Preparation and characterization of nanostructured CuO thin films using sol-gel dip coating*. in *IOP Conference Series: Materials Science and Engineering*. 2015. IOP Publishing. http://dx.doi.org/10.1088/1757-899X/99/1/012007

[25] V Dhanasekaran, N Soundaram, Seong-Il Kim, R Chandramohan, Srinivas Mantha, S Saravanakumar, and T Mahalingam. "Optical, electrical and microstructural studies of monoclinic CuO nanostructures synthesized by a sol–gel route." *New Journal of Chemistry* 38, no. 6 (2014): 2327-2333. http://dx.doi.org/10.1039/C4NJ00084F

[26] MF Nurfazliana, SA Kamaraddin, N Nafarizal, H Saim, and MZ Sahdan. *Synthesis and characterization of cupric oxide thin films by sol-gel method*. in *2014 IEEE International Conference on Semiconductor Electronics (ICSE2014)*. 2014. IEEE. http://dx.doi.org/10.1109/SMELEC.2014.6920805

[27] Maryam Bibi, Hussain Abbas, and Sabah Baqi. "Outcome of temperature variation on sol-gel prepared CuO nanostructure properties (optical and dielectric)." *Materials Chemistry and Physics* 192 (2017): 67-71. https://doi.org/10.1016/j.matchemphys.2017.01.074

[28] C. Yang, F. Xiao, J. Wang, and X. Su. "3D flower- and 2D sheet-like CuO nanostructures: Microwave-assisted synthesis and application in gas sensors." *Sensors and Actuators, B: Chemical* 207, no. Part A (2015): 177-185 DOI: 10.1016/j.snb.2014.10.063. https://doi.org/10.1016/j.snb.2014.10.063

[29] Liqing Liu, Kunquan Hong, Tengteng Hu, and Mingxiang Xu. "Synthesis of aligned copper oxide nanorod arrays by a seed mediated hydrothermal method." *Journal of alloys and compounds* 511, no. 1 (2012): 195-197. https://doi.org/10.1016/j.jallcom.2011.09.028

[30] Jaejin Oh, Hyukhyun Ryu, and Won-Jae Lee. "Effects of Fe doping on the photoelectrochemical properties of CuO photoelectrodes." *Composites Part B: Engineering* 163 (2019): 59-66. https://doi.org/10.1016/j.compositesb.2018.11.041